

# A novel soft information algorithm for closest point search in lattices with Tanner graph representations

Dumitru Mihai Ionescu, *Senior Member, IEEE*, Haidong Zhu, *Student Member, IEEE*

## Abstract

An efficient, low-complexity, soft-information detector for multiple input multiple output channels and lattice constellations was devised, based on Tanner graph representations of lattices. Due to the coding gain associated with a lattice, structural relations exist between certain lattice points, which can be associated via an equivalence relation for detection purposes. The algorithm can generate both total and extrinsic a posteriori probability at detector's output. The step-back artifact (of traditional sphere decoders) is eliminated. The algorithm applies to general lattices and enables iterative receivers; it was tested in the case of uncoded transmission for a superorthogonal constellation in two scenarios. In quasistatic (block) fading it was found to achieve maximum likelihood performance even with one 'surviving' label (out of six); in independent fading with coordinate (component) interleaving and iterations between equalization and detection, it performs close to interference-free transmission. The coordinate interleaved scenario outperforms former despite absence of forward error correction coding.

## Index Terms

Belief propagation on a lattice, sphere decoder, soft information lattice detection, closest point search in lattices, Tanner graph, MIMO, iterations detector-decoder.

## I. INTRODUCTION

Multiple input multiple output (MIMO) transmission has emerged as a strong scenario for future high-speed wireless communications due to the large capacity potential of MIMO channels. Space-time codes that exploit both spatial diversity and time diversity have been widely proposed as MIMO modulation in the past decade to achieve reliable transmission.

Recently, the importance of lattice MIMO constellations in constructing space-time lattice codes was recognized by El-Gamal *et al.* [10] from a diversity-multiplexing tradeoff perspective. Superorthogonal space-time codes—reported in [2], then in [3], [4], [5], [6] (where they were dubbed 'superorthogonal')—are in fact lattice space time codes; the lattice structure inherent to the superorthogonal construction was noted by Ionescu and Yan [7, Section III] (Example 2 in the sequel offers more detail). As lattices, such constellations lend themselves to efficient detection algorithms, e.g. sphere decoding. Classic sphere decoding (see [15] and references therein) use hard decision, along

with a step-back provision; soft-output versions have been imagined, but rely on a list of important candidates, and retain the step-back provision. In [1], lattice partitioning is used to divide the infinite lattice into a finite number of cosets. Each coset is then labeled by a codeword of a finite Abelian group block code, called a label code. In [13], a Tanner graph (TG) representation for the label code was developed; this opens an opportunity for using belief propagation on the lattice labels.

The sequel takes a novel, qualitatively different approach to soft-output closest point search in lattices, via a form of belief propagation on a lattice. Due to the coding gain associated with a lattice, structural relations exist between certain lattice points, which can be associated via an equivalence relation for detection purposes. The algorithm can generate both total and extrinsic *a posteriori* probability (APP) at the detector's output. The step-back feature is eliminated. For each channel use, a filter bank for interference cancellation with minimum mean square error (IC-MMSE) is used to remove the channel effects. Then, a reduced-complexity lattice decoder based on TG lattice representation is proposed for computing total APP and extrinsic APP. The capability of calculating the extrinsic APP enables decoding schemes that iterate between detection and decoding. This novel lattice detection algorithm is applied to detecting superorthogonal space-time lattice codes [7] in quasistatic fading, and to a coordinate interleaved [18] scenario. The following notation is adhered to. Vectors are denoted by lowercase bold letters;  $a_i$  denotes the  $i$ -th element of vector  $\mathbf{a}$ . Matrices are denoted by uppercase bold letters. The  $i$ -th column vector and the  $ij$ -th element of a matrix, say  $\mathbf{A}$ , are denoted by  $\mathbf{a}_i$  and  $a_{ij}$ , respectively. The superscripts T and H are used to denote transposition and complex conjugated transposition, respectively.

## II. PROBLEM DEFINITION AND SYSTEM MODEL

Complex and real transmission models are described; a general formulation for lattice constellations for MIMO channels is then introduced, followed by two examples pertaining respectively to linear dispersion and superorthogonal codes.

### A. Rayleigh flat fading MIMO channels

Consider MIMO wireless transmission with  $N_t$  transmit antennas and  $N_r$  receive antennas in Rayleigh flat fading. The channel coefficients are assumed to be constant over a block of  $T$  MIMO channel uses and change independently from block to block. The transmission of each block is then given by

$$\mathbf{Y} = \sqrt{1/N_t} \mathbf{S} \bar{\mathbf{H}} + \mathbf{N} \quad (1)$$

where  $\mathbf{Y} \in \mathbb{C}^{T \times N_r}$ ,  $\bar{\mathbf{H}} \in \mathbb{C}^{N_t \times N_r}$ ,  $\mathbf{S} \in \mathcal{A}^{T \times N_t}$  and  $\mathbf{N} \in \mathbb{C}^{T \times N_r}$  are *arrays* of received signals, channel gain coefficients, transmitted signals and additive noises, respectively. The elements of  $\mathbf{N}$  are i.i.d. zero-mean complex-valued Gaussian random variables with variance  $N_0/2$  per dimension, i.e.,  $n_{ij} \sim \mathcal{CN}(0, N_0)$ . The channel gain matrix  $\bar{\mathbf{H}}$  has elements  $\bar{h}_{ij} \sim \mathcal{CN}(0, 1)$  representing the channel gain coefficients between the  $i$ -th transmit antenna and the  $j$ -th receive antenna, assumed pairwise independent. The array  $\mathbf{S}$  describes the transmitted symbols chosen

from alphabet  $\mathcal{A}^1$ ;  $s_{ij} \in \mathbb{C}$  is radiated from the  $j$ -th transmit antenna during the  $i$ -th channel use. By enforcing the power constraint

$$\mathbb{E} \left\{ \frac{1}{T} \|\mathbf{S}\|^2 \right\} \leq N_t, \quad (2)$$

where  $\|\cdot\|$  denotes the Euclidean matrix norm and  $\mathbb{E}\{\cdot\}$  denotes expectation, the *average* signal-to-noise (SNR) ratio per receive antenna is  $1/N_0$ .

It is important to note that (1) can accommodate various setups, which include the case  $T = 1$  that allows for independent (rather than block) fading. Similarly, the arrays  $\mathbf{S}$  may have a certain structure, e.g. they may represent space-time code matrices; or, they may simply be arrays of unrelated values obtained after interleaving the real coordinates of structured matrices (Section IV-B) then forming new complex valued arrays out of the scrambled coordinates.

### B. Equivalent real-valued transmission model

Eq. (1) is the receive equation for the transmission of complex valued arrays from  $N_t$  transmit antennas during  $T$  MIMO channel uses. It is also convenient to introduce equivalent real-valued transmission models. To this end, define two isomorphisms from complex domain to real domain,  $\mathcal{I} : \mathbb{C}^M \mapsto \mathbb{R}^{2M \times 1}$  and  $\phi : \mathbb{C}^{M \times N} \mapsto \mathbb{R}^{2MN \times 1}$ , as follows:

$$\mathcal{I}(\mathbf{a}) \stackrel{\text{def}}{=} [\Re(\mathbf{a})^T \Im(\mathbf{a})^T]^T, \quad (3)$$

$$\phi(\mathbf{A}) \stackrel{\text{def}}{=} [\mathcal{I}(\mathbf{a}_1)^T \cdots \mathcal{I}(\mathbf{a}_N)^T]^T, \quad (4)$$

where  $\mathbf{a} \in \mathbb{C}^{M \times 1}$  and  $\mathbf{A} = [\mathbf{a}_1 \dots \mathbf{a}_N] \in \mathbb{C}^{M \times N}$ . The real-valued transmission model that is equivalent to (1) is

$$\mathbf{y}^c = \mathbf{H}^c \mathbf{x} + \mathbf{n}^c \quad (5)$$

where  $\mathbf{y}^c \stackrel{\text{def}}{=} \phi(\mathbf{Y}^T)$ ,  $\mathbf{n}^c \stackrel{\text{def}}{=} \phi(\mathbf{N}^T)$ ,  $\mathbf{x} \stackrel{\text{def}}{=} \phi(\mathbf{S}^T)$  and  $\mathbf{H}^c \stackrel{\text{def}}{=} \mathbf{I}_T \otimes \left( \begin{bmatrix} \Re(\bar{\mathbf{H}}^T) & -\Im(\bar{\mathbf{H}}^T) \\ \Im(\bar{\mathbf{H}}^T) & \Re(\bar{\mathbf{H}}^T) \end{bmatrix} \right)$ . Note that  $\mathbf{H}^c$  is a  $2N_r T \times 2N_t T$  block-diagonal real channel matrix consisting of  $T$  identical diagonal replicas the same  $2N_r \times 2N_t$  matrix ( $\mathbf{I}_T$  is the identity matrix of dimension  $T$  and  $\otimes$  denotes the Kronecker product). A similar model has been reported in [10].

In addition, define a new vector  $\mathbf{y} = \phi(\mathbf{Y})$ . By definition of  $\phi$ , it can be seen that the vector  $\mathbf{y}$  is some permutation  $\pi$  of  $\mathbf{y}^c$ , since  $\mathbf{y}$  and  $\mathbf{y}^c$  are isomorphisms, via  $\phi$ , of  $\mathbf{Y}$  and its transpose  $\mathbf{Y}^T$ . One can obtain  $\mathbf{y}$  from  $\mathbf{y}^c$  as follows:

$$\mathbf{y} = \pi(\mathbf{y}^c) = \pi(\mathbf{H}^c \mathbf{x} + \mathbf{n}^c) = \pi(\mathbf{H}^c) \mathbf{x} + \pi(\mathbf{n}^c) = \mathbf{H} \mathbf{x} + \mathbf{n}, \quad (6)$$

where  $\pi(\mathbf{H}^c) \stackrel{\text{def}}{=} \mathbf{H}$  denotes a row permutation of  $\mathbf{H}^c$  by  $\pi$ .

<sup>1</sup>Different alphabets could be used on different transmit antennas, e.g.  $\mathcal{A}_j$  could be used on the  $j$ -th transmit antenna; the alphabets  $\mathcal{A}_j$  could differ, for example, when identical constellations are assigned with unequal powers to different transmit antennas. While this general case could be accommodated it is secondary in importance for the purpose of this work.

The real channel models (6) and (5) are both equivalent to the MIMO model in eq. (1), and can be used interchangeably. In the sequel, (6) will be preferred since it is consistent with the transmission model used in [7]—which is referenced in order to address certain important properties of super-orthogonal space-time codes used, in turn, to demonstrate the algorithm for finding the closest point in a lattice.

### C. Space-time lattice codes

An  $m$ -dimensional real lattice  $\Lambda$  is a discrete additive subgroup of  $\mathbb{R}^m$  defined as  $\Lambda = \{\mathbf{B}\mathbf{u} : \mathbf{u} \in \mathbb{Z}^m\}$  where the real matrix  $\mathbf{B}$  of size  $m \times m$  is the generator matrix of  $\Lambda$  [10]. A lattice code  $\mathcal{C}(\Lambda, \mathbf{u}_0, \mathcal{R})$  is the finite subset of the lattice translate  $\Lambda + \mathbf{u}_0$  inside some shaping region  $\mathcal{R}$ , i.e.,  $\mathcal{C}(\Lambda, \mathbf{u}_0, \mathcal{R}) = \{\Lambda + \mathbf{u}_0\} \cap \mathcal{R}$ , where  $\mathcal{R}$  is a bounded region of  $\mathbb{R}^m$  [10]. A space-time coding scheme with a space-time code matrix set  $\mathcal{S}$ , such that  $\phi(\mathbf{S}^T) \in \mathbb{R}^m$  for all  $\mathbf{S} \in \mathcal{S}$ , is a lattice space-time code if the  $m$ -dimensional image of  $\mathcal{S}$  via the isomorphism  $\phi$  is a lattice code  $\mathcal{C}(\Lambda, \mathbf{u}_0, \mathcal{R})$ , i.e.,  $\phi(\{\mathcal{S}^T\}) = \{\{\mathbf{B}\mathbf{u} : \mathbf{u} \in \mathbb{R}^m\} + \mathbf{u}_0\} \cap \mathcal{R}$ . Many well-known space-time modulation schemes in the literature indeed can be treated as space-time lattice codes. Two important examples of space-time lattice codes are given below.

*Example 1: (Linear dispersion codes)* A linear dispersion code [11] defines a mapping of a complex vector  $\mathbf{s} = [s_0, s_1, \dots, s_{K-1}]^T$  to a  $T \times N_t$  complex matrix  $\mathbf{S}$  as follows:

$$\mathbf{S} = \sum_{l=0}^{K-1} (s_l \mathbf{P}_l + s_l^H \mathbf{Q}_l) \quad (7)$$

where  $\{\mathbf{P}_l\}_{l=0}^{K-1}, \{\mathbf{Q}_l\}_{l=0}^{K-1}$  are  $T \times N_t$  complex matrices. The linear dispersion code can be further rearranged as

$$\mathbf{S} = \sum_{l=0}^{K-1} \left( \Re(s_l) \tilde{\mathbf{P}}_l + \Im(s_l) \tilde{\mathbf{Q}}_l \right) \quad (8)$$

with  $\tilde{\mathbf{P}}_l = \mathbf{P}_l + \mathbf{Q}_l$  and  $\tilde{\mathbf{Q}}_l = i\mathbf{P}_l - i\mathbf{Q}_l$ . Let  $\boldsymbol{\chi} = \mathcal{I}(\mathbf{s})$ ; then one can express the linear dispersion code linearly in terms of  $\boldsymbol{\chi}$  and a set of matrices  $\mathcal{C} \stackrel{\text{def}}{=} \{\mathbf{C}_l\}_{l=0}^{2K-1} = \{\tilde{\mathbf{P}}_0, \tilde{\mathbf{P}}_1, \dots, \tilde{\mathbf{P}}_{K-1}, \tilde{\mathbf{Q}}_0, \tilde{\mathbf{Q}}_1, \dots, \tilde{\mathbf{Q}}_{K-1}\}$  via

$$\mathbf{S} = \sum_{i=0}^{2K-1} \chi_i \mathbf{C}_i, \quad (9)$$

where  $\mathbf{C}_i$  is the  $i$ -th matrix of  $\mathcal{C}$ . Consequently, the isomorphism of  $\mathbf{S}^T$  via  $\phi$ , denoted  $\mathbf{x}$ , is given by

$$\mathbf{x} \stackrel{\text{def}}{=} \phi(\mathbf{S}^T) = \sum_{i=0}^{2K-1} \chi_i \phi(\mathbf{C}_i^T) = \mathbf{\Gamma} \boldsymbol{\chi} \quad (10)$$

with  $\mathbf{\Gamma} = [\phi(\mathbf{C}_0^T), \dots, \phi(\mathbf{C}_{2K-1}^T)]$ .

It is clear from (10) that when the vector  $\boldsymbol{\chi}$  is proportional to a vector of integers a linear dispersion code is a lattice code with generator matrix  $\mathbf{\Gamma}$ ; this is the case when  $\mathbf{s}$  is from a particular modulation constellation such as PAM or QAM. In general,  $\boldsymbol{\chi}$  is not an integer vector, e.g. when the elements of  $\mathbf{s}$  are from a PSK constellation. However, if, by construction of the linear dispersion code,  $\mathbf{s}$  is selected to be from a lattice  $\Lambda'$  then the points  $\boldsymbol{\chi}$  are carved from the lattice  $\Lambda'$  via a shaping region  $\mathcal{R} \in \mathbb{R}^m$ . That is,

$$\boldsymbol{\chi} \in \Lambda' \cap \mathcal{R} \quad (11)$$

where  $\Lambda' = \{\mathbf{B}\mathbf{u} : \mathbf{u} \in \mathbb{Z}^m\}$  and  $\mathbf{B}$  is the generator matrix of  $\Lambda'$ , and the linear dispersion code is a lattice space-time code with generator matrix  $\mathbf{\Gamma}\mathbf{B}$ . One may find different pairs of lattice  $\Lambda'$  and shaping region  $\mathcal{R}$  defining

the same  $\chi$ s; the choice of  $\Lambda'$  and  $\mathcal{R}$  will influence the complexity of the corresponding decoder, as discussed in [13] (unless some basis reduction approach is used to process the generator matrix). The real transmission model becomes

$$\mathbf{y} = \mathbf{H}\mathbf{\Gamma}\mathbf{B}\mathbf{u} + \mathbf{n}, \quad (12)$$

and is equivalent to using a lattice space-time code with generator matrix  $\mathbf{\Gamma}\mathbf{B}$ .

*Example 2: (Super orthogonal space-time lattice codes)* A super-orthogonal space-time code is constructed [7] by expanding a (generalized) orthogonal design [8], which in turn is obtained as a linear combination of matrices similar to (7), (8), with expansion coefficients derived from a complex vector  $\mathbf{s}$ ; the difference from a linear dispersion code is that the latter matrices verify an additional constraint (see [7, eqs. (2), (3)]). A super-orthogonal space-time construction for  $T = 2$ ,  $N_t = 2$ , and QPSK constellation, having thirty two codematrixes, was described in [2], [3], [4], [5], [6]. A generic codematrix  $\mathbf{S}$  can be expressed as [7]<sup>2</sup>

$$\mathbf{S} = \sum_{l=0}^3 \chi_l \mathbf{C}_l + \sum_{l=0}^3 \chi'_l \mathbf{C}'_l, \quad (13)$$

$$\chi_l \neq 0 \Rightarrow \chi'_l = 0 \text{ and } \chi'_l \neq 0 \Rightarrow \chi_l = 0, \forall l; \quad (14)$$

above,  $\chi_l$  and  $\chi'_l$  ( $l = 0, 1, 2, 3$ ) are either 1,  $-1$ , or 0 and the nonzero values are real parts of complex elements from a complex QPSK constellation; the two sets of real coefficients  $\chi_l$  and  $\chi'_l$  ( $l = 0, 1, 2, 3$ ) are not simultaneously nonzero, i.e. either all  $\chi_l$ s or all  $\chi'_l$ s vanish. As discussed in [7], the super-orthogonal matrix codebook is embedded into an 8-dimensional real vector space obtained as the direct sum of two 4-dimensional real vector spaces<sup>3</sup>. The two sets of matrices  $\mathbf{C}_l$  and  $\mathbf{C}'_l$  are basis matrices in the component vector spaces that form the direct sum:

$$\mathbf{C} = \left\{ \begin{bmatrix} 1 & 0 \\ 0 & -1 \end{bmatrix}, \begin{bmatrix} 0 & 1 \\ 1 & 0 \end{bmatrix}, \begin{bmatrix} i & 0 \\ 0 & i \end{bmatrix}, \begin{bmatrix} 0 & -i \\ i & 0 \end{bmatrix} \right\}, \quad (15)$$

$$\mathbf{C}' = \left\{ \begin{bmatrix} 1 & 0 \\ 0 & 1 \end{bmatrix}, \begin{bmatrix} 0 & -1 \\ 1 & 0 \end{bmatrix}, \begin{bmatrix} i & 0 \\ 0 & -i \end{bmatrix}, \begin{bmatrix} 0 & i \\ i & 0 \end{bmatrix} \right\}. \quad (16)$$

The isomorphism of a super-orthogonal space-time codematrix  $\mathbf{S}$ , denoted by  $\mathbf{x} = \phi(\mathbf{S}^T)$ , is given by

$$\mathbf{x} = \phi(\mathbf{S}^T) = \mathbf{\Gamma}\boldsymbol{\chi}_{\oplus} \quad (17)$$

where  $\boldsymbol{\chi}_{\oplus} = [\chi_0, \chi_1, \dots, \chi_3, \chi'_0, \chi'_1, \dots, \chi'_3]^T = [\boldsymbol{\chi}^T \boldsymbol{\chi}'^T]^T \in \mathbb{R}^8$  is a direct sum of two 4-dimensional vectors, and  $\mathbf{\Gamma} = [\mathbf{\Gamma}_1 \mathbf{\Gamma}_2]$  is a  $8 \times 8$  real matrix with  $\mathbf{\Gamma}_1 = [\phi(\mathbf{C}_0^T), \dots, \phi(\mathbf{C}_3^T)]$  and  $\mathbf{\Gamma}_2 = [\phi(\mathbf{C}'_0^T), \dots, \phi(\mathbf{C}'_3^T)]$ , respectively. It also follows from [7] that  $\mathbf{\Gamma}$  is proportional with a unitary matrix via  $\mathbf{\Gamma}\mathbf{\Gamma}^H = 2\mathbf{I}_8$ .

<sup>2</sup> Definition (3) of the isomorphism  $\mathcal{I}$  from a complex vector to a real vector differs slightly from [7], where it was defined by interlacing the real and imaginary parts; i.e., in [7], if  $\mathbf{s} = [z_1, \dots, z_K]^T \in \mathbb{C}^K$  then  $\mathcal{I}(\mathbf{s}) = \boldsymbol{\chi} \stackrel{\text{def}}{=} [\Re\{z_1\}, \Im\{z_1\}, \dots, \Re\{z_K\}, \Im\{z_K\}]^T$ —rather than keeping the real (and imaginary) parts together as done in eq. (3). This is the reason for swapping the second and third matrices in eqs. (15), (16) relative to [7, Sec. III].

<sup>3</sup>In the superorthogonal construction the two 4-dimensional components of the direct sum are reflection symmetries (around origin) of one another [9].

Because  $\mathbf{s}$  takes values from a QPSK constellation  $\{\pm 1 \pm j\}$ ,  $j \stackrel{\text{def}}{=} \sqrt{-1}$ , the nonzero realizations of either of the two vectors  $\boldsymbol{\chi}, \boldsymbol{\chi}'$  are the sixteen 4-dimensional real vectors with elements  $\pm 1$ ; that is, either  $\boldsymbol{\chi}_\oplus = [\boldsymbol{\chi}^T [0\ 0\ 0\ 0]^T]^T$  or  $\boldsymbol{\chi}_\oplus = [[0\ 0\ 0\ 0]^T \boldsymbol{\chi}'^T]^T$ .

Since  $\boldsymbol{\chi}_\oplus \in \mathbb{Z}^8$ , the vector  $\boldsymbol{x}$  is recognized to be from some lattice  $\Lambda$  with generator matrix  $\boldsymbol{\Gamma}$ , via (17). In the sequel it is helpful to further recognize that  $\boldsymbol{\chi}_\oplus$  itself is from a direct sum a two 4-dimensional checkerboard lattices. Indeed, consider the lattice  $L \stackrel{\text{def}}{=} D_4 \oplus D_4$ ; i.e., a point  $[\lambda_1\ \lambda_2\ \dots\ \lambda_8]$  in  $D_4 \oplus D_4$  has the property that  $[\lambda_1\ \lambda_2\ \lambda_3\ \lambda_4], [\lambda_5\ \lambda_6\ \lambda_7\ \lambda_8]$  are from  $D_4$ . Let  $[d_1\ d_2\ d_3\ d_4]$  denote a point in the second shell of  $D_4$ , i.e. satisfying  $\sum_{i=1}^4 d_i^2 = 4$ . There are twenty four points in the second shell of  $D_4$ , of which exactly sixteen will satisfy  $|d_i| = 1$ ; denote this set by  $\mathcal{D}$ . If  $\boldsymbol{B}$  is the  $4 \times 4$  generator matrix of  $D_4$  then  $D_4 \oplus D_4$  has generator matrix  $\begin{bmatrix} \boldsymbol{B} & \mathbf{0}_{4 \times 4} \\ \mathbf{0}_{4 \times 4} & \boldsymbol{B} \end{bmatrix}$ . Then  $L = L_1 \oplus L_2$ , where  $L_1$  and  $L_2$  have generator matrices  $[\boldsymbol{B}\ \mathbf{0}_{4 \times 4}]$  and respectively  $[\mathbf{0}_{4 \times 4}\ \boldsymbol{B}]$ . Both  $L_1$  and  $L_2$  are isomorphic with  $D_4$ .  $L_1$  contains the sixteen points in the set  $\left\{ [c^T [0\ 0\ 0\ 0]^T]^T \mid c \in \mathcal{D} \right\}$ , and  $L_2$  contains the sixteen points in the set  $\left\{ [0\ 0\ 0\ 0]^T c^T \mid c \in \mathcal{D} \right\}$ . Note that the nonzero realizations of either of the vectors  $\boldsymbol{\chi}, \boldsymbol{\chi}'$  are the sixteen points in the second shell of  $D_4$  having unit magnitude real coordinates; thereby,  $\Lambda = \Lambda_1 \oplus \Lambda_2$  where  $\Lambda_i$  is isomorphic with  $L_i$ ,  $i = 1, 2$ , and  $\boldsymbol{\chi}_\oplus$  is from a direct sum a two 4-dimensional checkerboard lattices. A generator matrix for a checkerboard lattice  $D_4$  is, e.g., the matrix  $\boldsymbol{B}$  in (35).

It follows from (17) that  $\boldsymbol{x} = \phi(\boldsymbol{S}^T)$  can be written as

$$\boldsymbol{x} = \boldsymbol{\Gamma} \boldsymbol{\chi}_\oplus = \boldsymbol{\Gamma} \begin{bmatrix} \boldsymbol{B} & \mathbf{0}_{4 \times 4} \\ \mathbf{0}_{4 \times 4} & \boldsymbol{B} \end{bmatrix} \boldsymbol{u}, \quad \boldsymbol{u} = [u_1 \dots u_4]^T \in \mathbb{Z}^4 \quad (18)$$

where  $\boldsymbol{B}$  is the generator matrix of the checkerboard lattice  $D_4$ , given in (35). Thereby,  $\boldsymbol{x}$  can be viewed as being from a lattice with generator matrix  $\boldsymbol{\Gamma} \begin{bmatrix} \boldsymbol{B} & \mathbf{0}_{4 \times 4} \\ \mathbf{0}_{4 \times 4} & \boldsymbol{B} \end{bmatrix} = [\boldsymbol{\Gamma}_1 \boldsymbol{B} \ \boldsymbol{\Gamma}_2 \boldsymbol{B}]$ .

For a super-orthogonal space-time lattice code the real equivalent transmission model in eq. (6) becomes

$$\boldsymbol{y} = \boldsymbol{H} \boldsymbol{x} + \boldsymbol{n} = \boldsymbol{H} \boldsymbol{\Gamma} \boldsymbol{\chi}_\oplus + \boldsymbol{n} = \boldsymbol{H}_\oplus \boldsymbol{\chi}_\oplus + \boldsymbol{n} = \boldsymbol{H}_\oplus \boldsymbol{B} \boldsymbol{u} + \boldsymbol{n} \quad (19)$$

where the second equality is obtained according to (17), and  $\boldsymbol{H}_\oplus \stackrel{\text{def}}{=} \boldsymbol{H} \boldsymbol{\Gamma}$ . Note that in [7] the transmission model for the same super-orthogonal space-time code is (see footnote 2):

$$\boldsymbol{y}_\oplus = \boldsymbol{G}_\oplus \boldsymbol{\chi}_\oplus + \boldsymbol{n}_\oplus. \quad (20)$$

It can be verified that  $\boldsymbol{G}_\oplus = \begin{bmatrix} \boldsymbol{H} \boldsymbol{\Gamma}_1 & \mathbf{0}_{4 \times 4} \\ \mathbf{0}_{4 \times 4} & \boldsymbol{H} \boldsymbol{\Gamma}_2 \end{bmatrix}$ . Furthermore, the matrix  $\boldsymbol{G}_\oplus$  was shown in [7] to be proportional with a unitary matrix, i.e.,  $\boldsymbol{G}_\oplus \boldsymbol{G}_\oplus^H = \alpha \boldsymbol{I}$ . Denote  $\boldsymbol{H}_\oplus^1 \stackrel{\text{def}}{=} \boldsymbol{H} \boldsymbol{\Gamma}_1$  and  $\boldsymbol{H}_\oplus^2 \stackrel{\text{def}}{=} \boldsymbol{H} \boldsymbol{\Gamma}_2$ . Then,  $\boldsymbol{H}_\oplus^k$ ,  $k = 1, 2$ , is unitary up to a scalar, i.e.

$$\boldsymbol{H}_\oplus^k \boldsymbol{H}_\oplus^k{}^H = \alpha \boldsymbol{I}, \quad k = 1, 2. \quad (21)$$

### III. REDUCED SEARCH SOFT-OUTPUT DETECTOR FOR CLOSEST POINT SEARCH IN LATTICES

While lumping a channel matrix with some (equivalent) generator matrix—as in (19)—might be tempting, the new lattice having generator matrix  $\boldsymbol{H} \boldsymbol{\Gamma}$  or  $\boldsymbol{H} \boldsymbol{\Gamma} \boldsymbol{B}$  may have labels with very large label coordinate alphabets (see Section III-B, [13]) for random  $\boldsymbol{H}$ —unless some form of basis reduction can be devised. It is more straightforward

to illustrate the concept by removing the effect of the channel matrix  $\mathbf{H}$  via some equalization step, then dealing with the underlying lattice separately. This is the approach taken in the sequel.

A novel soft-information detection algorithm for lattice space-time constellations is introduced below. Detection is performed in two stages: linear minimum mean square error (LMMSE) filtering, and belief propagation (BP) on a lattice. In the first stage, a finite impulse response (FIR) LMMSE filter bank is used to remove the effect of the channel; the lattice redundancy is subsequently exploited by a novel lattice detector based on a Tanner graph representation of the lattice.

#### A. MMSE soft equalizer with interference cancellation

The equivalent real transmission model is given in (6). The goal of the MMSE soft equalizer is to remove the effect of the channel  $\mathbf{H}$ , and provide a soft estimate of each component  $x_i$  of  $\mathbf{x}$  so as to minimize the interference due to other coordinates  $\{x_l\}_{l=1, l \neq i}^{2N_t T}$ , and to noise  $\mathbf{n}$ . For the  $i$ -th branch, the soft estimate, denoted as  $\hat{x}_i$ , is given by

$$\hat{x}_i = \mathbf{m}_i^T \mathbf{y} \quad (22)$$

with the  $i$ -th FIR filter  $\mathbf{m}_i$  being

$$\mathbf{m}_i = \arg \min_{\mathbf{m} \in \mathbb{R}^{2N_t T \times 1}} \mathbb{E} \{ \|x_i - \mathbf{m}^T \mathbf{y}\|^2 \} \quad (23)$$

subject to the unit power constraint

$$\mathbf{m}_i^T \mathbf{h}_i = 1. \quad (24)$$

This power constraint mitigates the attenuation effect on the desired signal due to the filtering. The optimal solution is [12]

$$\mathbf{m}_i = \mathbf{m}_i^c + \frac{a_i}{\mathbf{h}_i^T \mathbf{R}^{-1} \mathbf{h}_i} \mathbf{R}^{-1} \mathbf{h}_i \quad (25)$$

where  $\mathbf{R} = \frac{P}{2N_t} \mathbf{H} \mathbf{H}^H + \frac{N_0}{2} \mathbf{I}$  is the covariance matrix of  $\mathbf{y}$ ,  $\mathbf{m}_i^c = \frac{P}{2N_t} \mathbf{R}^{-1} \mathbf{h}_i$  is the optimal solution for (23) without power constraint, and  $a_i = 1 - \mathbf{m}_i^c \mathbf{h}_i$ . The MSE  $\sigma_i^2 = \mathbb{E} \{ \|x_i - \mathbf{m}_i^T \mathbf{y}\|^2 \}$  of the  $i$ -th branch is

$$\sigma_i^2 = \frac{P}{2N_t} - (\mathbf{m}_i^c)^T \mathbf{R} \mathbf{m}_i^c + \frac{a_i}{\mathbf{h}_i^T \mathbf{R}^{-1} \mathbf{h}_i} \quad (26)$$

If detection and decoding can be performed iteratively, then soft information about  $\mathbf{x}$  can be fed back from the FEC decoder and made available to the filter bank in the form of probabilities of valid realizations of transmitted vectors  $\mathbf{x}$ , or its elements  $x_i$ ; i.e. either at the vector level  $\mathbf{x}$ ,  $\{\Pr(\mathbf{x} = \phi(\mathbf{C}^T)) \mid \phi(\mathbf{C}^T) \in \mathcal{C}(\Lambda, \mathbf{u}_0, \mathcal{R})\}$ , or at the coordinate level—e.g. in the case when coordinate interleaving [18] is used to scramble the coordinates of several vectors  $\mathbf{x}$  prior to transmission. In the latter case the structure present in the different multidimensional lattice points is destroyed during transmission through the channel; not only does this mean that the coordinate probabilities supplied by the decoder have to be unscrambled before being fed back to the LMMSE filter for interference

cancellation (IC—see Fig. 4), but the performance can be improved (over the non-interleaved scenario) even in an uncoded system (see Section IV-B).

An iterative receiver aims at iteratively canceling the interference prior to filtering by forming a soft interference estimator in one of two ways:

1) *Vector level feedback*:

$$\mathbf{x}_{\text{IC}} = \sum_{\phi(\mathbf{C}^T) \in \mathcal{C}(\Lambda, \mathbf{u}_0, \mathcal{R})} \phi(\mathbf{C}^T) \Pr(\mathbf{x} = \phi(\mathbf{C}^T)) \quad (27)$$

2) *Coordinate level feedback*: If  $\mathcal{K}_i$  is the  $i$ th coordinate alphabet, the average interference value at position  $i$  is

$$x_{\text{IC},i} = \sum_{\zeta \in \mathcal{K}_i} \zeta \Pr(x_i = \zeta). \quad (28)$$

Let  $\mathbf{x}_{\text{IC},\bar{i}}$  denote the vector obtained by setting the  $i$ -th element of  $\mathbf{x}_{\text{IC}}$  to zero, i.e.,  $\mathbf{x}_{\text{IC},\bar{i}} = [\dots, x_{\text{IC},i-1}, 0, x_{\text{IC},i+1}, \dots]^T$ , the interference cancellation is performed for the  $i$ -th branch

$$\hat{\mathbf{y}}_i = \mathbf{y} - \mathbf{H} \mathbf{x}_{\text{IC},\bar{i}}, \quad (29)$$

and the soft estimate  $\hat{x}_i$  of the  $i$ -th branch after IC is

$$\hat{x}_i = \mathbf{m}_i^T \hat{\mathbf{y}}_i \quad (30)$$

subject to a unit power constraint like (24). The estimation (30) is referred to IC-MMSE. The covariance matrix of  $\hat{\mathbf{y}}_i$ , denoted as  $\mathbf{R}_{\text{IC},i}$ , is

$$\mathbf{R}_{\text{IC},i} = \mathbf{H} \mathbf{Q}_{\text{IC},i} \mathbf{H}^H + \frac{N_0}{2} \mathbf{I} \quad (31)$$

with  $\mathbf{Q}_{\text{IC},i} = \frac{P}{2N_i} \mathbf{I} - \text{diag}\{\mathbf{x}_{\text{IC},\bar{i}}\} \text{diag}\{\mathbf{x}_{\text{IC},\bar{i}}\}$ . Substituting  $\mathbf{R}_{\text{IC},i}$  of (31) for  $\mathbf{R}$  in (25), (26), yields the IC-MMSE solution  $\mathbf{m}_i$  and the corresponding MSE  $\sigma_i^2$ , respectively. Note that the IC-MMSE filter bank is a more general solution than a MMSE filter bank for removing channel effects in a MIMO scenarios. After IC-MMSE filtering the soft estimate of the  $i$ th branch is

$$\hat{x}_i = x_i + \hat{n}_i \quad (32)$$

with  $\hat{n}_i \sim \mathcal{N}(0, \sigma_i^2)$ , or written in a matrix form as

$$\hat{\mathbf{x}} = \mathbf{x} + \hat{\mathbf{n}}. \quad (33)$$

### B. Belief propagation detector for lattice code based on Tanner graph representation

After IC-MMSE equalization, the soft estimate  $\hat{\mathbf{x}}$  of a lattice point is obtained. Recall that in lattice space-time schemes, the codebook of transmitted vectors  $\mathbf{x}$  is a lattice code  $\mathcal{C}(\Lambda, \mathbf{u}_0, \mathcal{R})$ , where the generator matrix of  $\Lambda$  is  $\Gamma \mathbf{B}$ . For simplicity, let  $\mathbf{B}$  be a generic lattice generator matrix. Lattice detection is to either decide which lattice point *inside the shaping region* has the minimum distance to  $\hat{\mathbf{x}}$ , or calculate the soft information (e.g., in the form of probability or log-likelihood ratio) about each candidate lattice point. The first detection criterion leads to hard decision detectors—e.g., maximum likelihood (ML). The second decoding criterion leads to soft decision detectors,

which can be used in iterations between detection and decoding. In this section, a novel Tanner graph based lattice decoding algorithm is introduced. For simplicity, assume an  $m$ -dimensional lattice code, i.e.,  $\hat{\mathbf{x}} \in \mathbb{R}^m$ .

The novel lattice decoding algorithm introduced below relies on Tanner graph representations of lattices [13], which are enabled by lattice partitioning; all lattice points (those inside the shaping region are of interest) are partitioned into several subgroups (cosets). Each subgroup includes several different lattice points, and is labelled by a well-defined Abelian group block codeword. Then, a reduced-complexity soft-output lattice detector can be obtained by operating on the smaller number of cosets instead of lattice points. The labels of all cosets form an Abelian block code, which can be represented by a Tanner graph similar to low-density-parity-check (LDPC) codes. Belief propagation on a lattice is performed on its non-binary label Tanner graph to yield the total and extrinsic APP of the labels and their coordinates, as described in the following subsections. The APPs of individual lattice points are obtained in a final step described in Section III-D.

A somewhat subtler point is that lattice partitioning revolves around an orthogonal sublattice  $\Lambda'$  of  $\Lambda$ , and the quotient group  $\Lambda/\Lambda'$ ;  $|\Lambda/\Lambda'|$  is finite iff  $\Lambda$  and  $\Lambda'$  have the same dimensionality. The most straightforward way of obtaining  $\Lambda'$  is by G-S orthogonalization of  $\Lambda$ 's generator matrix, whereby all orthogonal G-S directions intercept  $\Lambda$  and the intersection naturally forms a sublattice of the same dimensionality as  $\Lambda$ ; in all other cases the orthogonal sublattice will have to be obtained by some means other than G-S orthogonalization.

1) *Gram-Schmidt (G-S) orthogonalization*: Given a generator matrix  $\mathbf{B} = [\mathbf{b}_1 \dots \mathbf{b}_m]$ , obtain a set of orthogonal vectors  $\{\mathbf{w}_i\}_{i=1}^m$ .<sup>4</sup> Let  $W_i$  denote the vector space spanned by  $\mathbf{w}_i$ , i.e.,  $W_i = \alpha \mathbf{w}_i, \forall \alpha \in \mathbb{R}$ ;  $\mathcal{S} \stackrel{\text{def}}{=} \{W_i\}_{i=1}^m$  is a coordinate system.

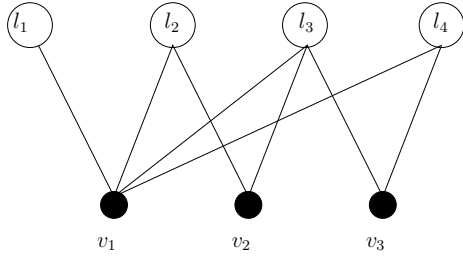
2) *Lattice label groups  $G_i$* : Let  $P_{W_i}(\Lambda)$  be the projection of  $\Lambda$  onto the vector space  $W_i$ , and  $\Lambda_{W_i} \stackrel{\text{def}}{=} \Lambda \cap W_i$ . The quotient group  $P_{W_i}(\Lambda)/\Lambda_{W_i}$  is called a label group  $G_i$ ;  $\Lambda$  is now partitioned into a finite set of cosets labeled by  $n$ -tuples from  $G \stackrel{\text{def}}{=} G_1 \times \dots \times G_m$ . The (finite) set of all label  $n$ -tuples, denoted  $L(\Lambda)$ , is called the label code, and uses  $G \stackrel{\text{def}}{=} G_1 \times \dots \times G_m$  as its alphabet space.

3) *Lattice label code  $L(\Lambda)$* : Due to the isomorphism  $G_i \cong \mathbb{Z}_{g_i}$ , with  $g_i \stackrel{\text{def}}{=} |G_i|$ , let  $G = \mathbb{Z}_{g_1} \times \dots \times \mathbb{Z}_{g_m}$ . A lattice point will be labeled by the label of the coset to which it belongs. The label code  $L(\Lambda)$  is an Abelian block code. Let  $\mathbf{l} = [l_1 \dots l_m]^T$  denote a label, and  $\Lambda(\mathbf{l})$  denote the set of lattice points sharing the label  $\mathbf{l}$ ; clearly, labeling is invariant to translations of  $\Lambda$  by  $\mathbf{u}_0$ . Let  $L(\Lambda)$ ,  $L(\mathcal{C}(\Lambda, \mathbf{u}_0, \mathcal{R}))$  denote the label codes of  $\Lambda$ , and of the subset of translated lattice points inside a shaping region  $\mathcal{R}$ , respectively. Then, a translated lattice point inside  $\mathcal{R}$  will have a label  $\mathbf{l} \in L(\mathcal{C}(\Lambda, \mathbf{u}_0, \mathcal{R}))$ .

4) *Finding a set of generator vectors  $\mathcal{V}^* \stackrel{\text{def}}{=} \{\mathbf{v}_i^*\}_{i=1}^n$  for the dual label code  $L(\Lambda)^*$  of  $\Lambda$ 's label code  $L(\Lambda)$*  [13]: The generator vectors  $\{\mathbf{v}_i^*\}_{i=1}^n$  characterize the lattice  $\Lambda$  like a parity check equation characterizes a linear block code, and have the following property: all the labels in  $L(\Lambda)$  are orthogonal to every vector  $\mathbf{v}_i$  in  $\{\mathbf{v}_i^*\}_{i=1}^n$ , i.e.,

$$\mathbf{v}_i^{*\text{T}} L(\Lambda) = 0 \text{ mod lcm}(g_1, g_2, \dots, g_m) \quad (34)$$

<sup>4</sup>Essentially,  $\mathbf{w}_1 = \mathbf{b}_1, \mathbf{w}_i = \mathbf{b}_i - \sum_{j=1}^{i-1} \mu_{ij} \mathbf{w}_j, i = 2, \dots, m$ , where  $\mu_{ij} = \langle \mathbf{b}_i, \mathbf{w}_j \rangle / \langle \mathbf{w}_j, \mathbf{w}_j \rangle$ , and  $\langle \cdot, \cdot \rangle$  denotes inner product.



$$3l_1 + l_2 + 5l_3 + 3l_4 = 0 \pmod{6} \mid l_2 + 2l_3 = 0 \pmod{3} \mid l_3 + l_4 = 0 \pmod{2}$$

Fig. 1. Tanner graph for Example 3, following [13].

where  $\text{lcm}(\cdot, \dots, \cdot)$  is the least common multiple.

5) *Lattice Tanner graph*: The generator vectors  $\{\mathbf{v}_i^*\}_{i=1}^n$  act as check equations for the label code  $L(\Lambda)$ , according to (34). Each coordinate of a label  $l$  corresponds to a variable node, and each generator vector that defines a check equation involving several label coordinates corresponds to a check node. A Tanner graph is constructed according to the constraints placed on label coordinates by the generator vectors  $\{\mathbf{v}_i^*\}_{i=1}^n$ . In general, the check equations are not over  $GF(2)$ , unless the cardinalities of the label groups  $G_i$  are all two. Thereby, the TG of a lattice is, generally, non-binary.

*Example 3*: ( $\Lambda = D_4$ ) A checkerboard lattice in  $\mathbb{R}^4$ , denoted  $D_4$ , has a matrix generator:

$$\mathbf{B} = \begin{bmatrix} 1 & 1 & 1 & 2 \\ 1 & 0 & 1 & 0 \\ 0 & 1 & 1 & 0 \\ 0 & 0 & 1 & 0 \end{bmatrix}. \quad (35)$$

The associated Gram-Schmidt vectors are

$$\begin{aligned} \mathbf{w}_1 &= [1, 1, 0, 0]^T \\ \mathbf{w}_2 &= [1/2, -1/2, 1, 0]^T \\ \mathbf{w}_3 &= [-1/3, 1/3, 1/3, 1]^T \\ \mathbf{w}_4 &= [1/2, -1/2, -1/2, 1/2]^T. \end{aligned} \quad (36)$$

In the coordinate system  $\{W_i\}_{i=1}^4 = \text{span}\{\mathbf{w}_i\}_{i=1}^4$ , we obtain the following projection and cross-section:

$$\begin{aligned} P_{W_1}(\Lambda) &= \frac{\mathbb{Z}}{\sqrt{2}} \frac{\mathbf{w}_1}{\|\mathbf{w}_1\|} & \Lambda_{W_1} &= \sqrt{2}\mathbb{Z} \frac{\mathbf{w}_1}{\|\mathbf{w}_1\|} \\ P_{W_2}(\Lambda) &= \frac{\mathbb{Z}}{\sqrt{6}} \frac{\mathbf{w}_2}{\|\mathbf{w}_2\|} & \Lambda_{W_2} &= \sqrt{6}\mathbb{Z} \frac{\mathbf{w}_2}{\|\mathbf{w}_2\|} \\ P_{W_3}(\Lambda) &= \frac{\mathbb{Z}}{\sqrt{3}} \frac{\mathbf{w}_3}{\|\mathbf{w}_3\|} & \Lambda_{W_3} &= 2\sqrt{3}\mathbb{Z} \frac{\mathbf{w}_3}{\|\mathbf{w}_3\|} \\ P_{W_4}(\Lambda) &= \mathbb{Z} \frac{\mathbf{w}_4}{\|\mathbf{w}_4\|} & \Lambda_{W_4} &= 2\mathbb{Z} \frac{\mathbf{w}_4}{\|\mathbf{w}_4\|}. \end{aligned}$$

This results in the following quotient groups for  $D_4$ :  $G_1(\Lambda) = \left\{0, \frac{\sqrt{2}}{2}\right\}$ ,  $G_2(\Lambda) = \left\{0, \frac{\sqrt{6}}{6}, \frac{\sqrt{6}}{3}, \frac{\sqrt{6}}{2}, \frac{2\sqrt{6}}{3}, \frac{5\sqrt{6}}{6}\right\}$ ,  $G_3(\Lambda) = \left\{0, \frac{\sqrt{3}}{3}, \frac{2\sqrt{3}}{3}, \sqrt{3}, \frac{4\sqrt{3}}{3}, \frac{5\sqrt{3}}{3}\right\}$ ,  $G_4(\Lambda) = \{0, 1\}$ . The label code and the dual label code  $L(\Lambda), L(\Lambda)^* \subset \mathbb{Z}_2 \times \mathbb{Z}_6 \times \mathbb{Z}_6 \times \mathbb{Z}_2$  are, respectively [13],

$$\begin{aligned} L(\Lambda) &= \{0000, 0031, 0220, 0251, 1300, 1331, \\ &\quad 1520, 1551, 1140, 1111, 0440, 0411\}, \\ L(\Lambda)^* &= \{0000, 0240, 0420, 1511, 1300, 1331, \\ &\quad 0451, 1540, 1151, 0031, 1120, 0211\}. \end{aligned}$$

The generator set for  $L(\Lambda)^*$  is  $\mathcal{V}^* = \{1151, 0240, 0031\}$ . Since  $\text{lcm}(g_1, g_2, g_3, g_4) = 6$ , the TG of label code  $L(\Lambda)$  can be constructed accordingly, as given in Fig. 1, where  $v_j$  is the  $j$ -th check node, and  $l_i$  is the  $i$ -th variable. The variable nodes associated with generator vector  $\mathbf{v}_j^*$  are connected to  $v_j$ ; e.g., check node  $v_1$  is connected to all four variable nodes, because all variable nodes are involved in the first check equation.

6) *Non-binary belief propagation* [14]:  $P_{W_i}(\hat{\mathbf{x}})$  denotes the projection of  $\hat{\mathbf{x}}$ , which may not be in  $\Lambda$ , onto vector space  $W_i$ , i.e.,  $P_{W_i}(\hat{\mathbf{x}}) = \hat{\mathbf{x}}^T \mathbf{w}_1 / \|\mathbf{w}_1\|$ . In the lattice Tanner graph a value  $\alpha \in \{0, 1, \dots, g_i - 1\}$  of the variable node  $l_i$  is associated with the hypothesis that  $\hat{\mathbf{x}}$  is an observation of a lattice point whose label has  $i$ -th coordinate equal to  $\alpha$  (or, whose projection on the vector space  $W_i$  belongs to coset with label  $\alpha$ );  $\Pr(l_i = \alpha)$  is the probability of this hypothesis.

Define messages  $q_{ji}^\alpha$  and  $r_{ji}^\alpha$  where the subscripts  $i, j$  refer to  $i$ -th variable node  $l_i$  and  $j$ -th check node  $v_j$ , respectively. The quantity  $q_{ji}^\alpha$  is the probability of the hypothesis that  $\hat{\mathbf{x}}$  is an observation of a lattice point whose label has  $i$ -th coordinate equal to  $\alpha$ , given the information obtained via check nodes other than  $v_j$ ;  $r_{ji}^\alpha$  is the probability of check  $v_j$  being satisfied given that  $\hat{\mathbf{x}}$  is an observation of a lattice point whose label has  $i$ -th coordinate equal to  $\alpha$ . The message passing is [14]:

$$r_{ji}^\alpha = \sum_{\substack{\mathbf{l} \in L(\Lambda), \\ \mathbf{v}_j^{*T} \mathbf{l} \equiv 0 \\ l_i = \alpha}} \prod_{k \in \mathcal{N}(j) \setminus i} q_{jk}^{l_k}, \quad (37)$$

$$q_{ji}^\alpha = K_{ji} f_i^\alpha \prod_{k \in \mathcal{M}(i) \setminus j} r_{ki}^\alpha, \quad (38)$$

where  $K_{ji}$  are so that  $\sum_{\alpha} q_{ji}^\alpha = 1$ ,  $\mathcal{N}(j)$  is the set of variable nodes involved in check equation  $v_j$ , and  $\mathcal{M}(i)$  is the set of checks nodes connected to variable node  $l_i$ ;  $f_i^\alpha$  is the initial probability of event  $l_i = \alpha$  given observation  $\hat{\mathbf{x}}$ .

### C. Initializing the lattice Tanner graph

Belief propagation requires initializing  $f_i^\alpha$  for the TG; this can be done in either projection domain or probability domain. After partitioning the infinite lattice into finitely many *labeled* cosets, not all labels are used by the points inside the finite shaping region; due consideration must be given to this aspect.

1) *In projection domain:* The soft estimate  $\hat{\mathbf{x}}$  obtained from the LMMSE filters bank is projected onto vector spaces  $\{W_i\}_{i=1}^m$  (see Fig. 2); in general,  $f_i^\alpha$  is initialized as:

(1).  $\forall \mathbf{l} \in L(\mathcal{C}(\Lambda, \mathbf{u}_0, \mathcal{R}))$ , find closest  $\lambda \in \mathcal{R} \cap \{\Lambda(\mathbf{l}) + \mathbf{u}_0\}$ :

$$\lambda_{\min}(\mathbf{l}) = \arg \min_{\lambda \in \Lambda(\mathbf{l})} \sum_{i=1}^m |P_{W_i}(\hat{\mathbf{x}}) - P_{W_i}(\lambda)|^2 \quad (39)$$

(2). Calculate the probability of (subgroup with) label  $\mathbf{l}$ :

$$\Pr(\mathbf{l}) = \frac{\exp\left(-\sum_{i=1}^m \frac{d_i^2(\lambda_{\min}(\mathbf{l}))}{2\sigma_i^2}\right)}{\sum_{\mathbf{l} \in L(\mathcal{C}(\Lambda, \mathbf{u}_0, \mathcal{R}))} \exp\left(-\sum_{i=1}^m \frac{d_i^2(\lambda_{\min}(\mathbf{l}))}{2\sigma_i^2}\right)}, \quad (40)$$

with  $d_i(\lambda_{\min}(\mathbf{l})) = |P_{W_i}(\hat{\mathbf{x}}) - P_{W_i}(\lambda_{\min}(\mathbf{l}))|$ , and  $\sigma_i^2$  of (26).

(3). Initialize  $f_i^\alpha$  from  $\Pr(\mathbf{l})$ :

$$f_i^\alpha = \sum_{\mathbf{l}: l_i = \alpha} \Pr(\mathbf{l}). \quad (41)$$

Then  $q_{ji}^\alpha$  is initialized to  $f_i^\alpha$ . The belief propagation algorithm is implemented by updating  $r_{ji}^\alpha$  and  $q_{ji}^\alpha$  iteratively until a predetermined number of iterations is achieved.

*Remark 1:* (Simplified initialization) One can examine  $\hat{\mathbf{x}}$  along each  $W_i$  separately—no precaution taken to verify that selecting the closest projection coordinate in each direction, in isolation from other directions, yields *collectively* a point inside the shaping region.

(1).  $\forall \mathbf{l}$ , the minimum distance  $d_i(\mathbf{l})$  along  $W_i$  is

$$d_i(\mathbf{l}) = \arg \min_{\lambda \in \Lambda(\mathbf{l})} |P_{W_i}(\hat{\mathbf{x}}) - P_{W_i}(\lambda)|. \quad (42)$$

(2). Calculate the probability of subgroup with label  $\mathbf{l}$  via

$$\Pr(\mathbf{l}) = \frac{\exp\left(-\sum_{i=1}^m \frac{d_i^2(\mathbf{l})}{2\sigma_i^2}\right)}{\sum_{\mathbf{l} \in L(\mathcal{C}(\Lambda, \mathbf{u}_0, \mathcal{R}))} \sum_{i=1}^m \exp\left(-\frac{d_i^2(\mathbf{l})}{2\sigma_i^2}\right)}.$$

Lastly,  $f_i^\alpha$  is initialized according to (41). This approach is referred to as simplified initialization, which is less complicated than the previous one—hence a slight performance loss.

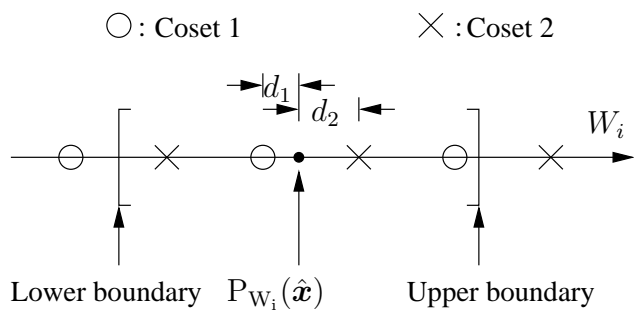


Fig. 2. Illustrative projection of a point  $\hat{\mathbf{x}} \in \mathbb{R}^m$  on one of the orthogonal directions  $W_i$ ,  $i = 1, \dots, m$ , whose label group has cardinality  $|G_i| = 2$ .

2) *In probability domain:* Given the soft estimates in  $\hat{\boldsymbol{x}}$ , the likelihoods of each coordinate<sup>5</sup> of  $\boldsymbol{x} \in \Lambda$  at the  $k$ -th MIMO channel use are calculated from the soft estimates in  $\hat{\boldsymbol{x}}$ <sup>6</sup>:

$$P(\hat{x}_i | x_i = c^j) = K \exp(-\|\hat{x}_i - c^j\|^2 / 2\sigma_i^2), \quad (43)$$

where  $c^j$  is the  $j$ -th real coordinate  $x_i$  of  $\boldsymbol{x} \in \Lambda \cap \mathcal{R}$ . Then, the likelihood of each value of coordinate  $x_i$  at the  $k$ -th MIMO channel use will form the component  $P_k(c^j; I)$  of a vector input  $P_k(\boldsymbol{c}; I)$  to a SISO APP module, following the model and notations in [16]; as in [16],  $C_k^j$  will denote a random process enacted by a sequence of (coordinate) symbols taking values from some alphabet  $\{c^j | j \in \mathcal{J}\}$ —which nonetheless may be nonbinary, i.e.  $j$  is from a set of cardinality  $|\mathcal{J}| > 2$ .

*D. Computation of extrinsic APP—either (lattice) point-wise or coordinate-wise—after belief propagation*

In order to implement iterative receivers it is necessary to compute the a posteriori probability at the end of belief propagation. After the last iteration, the belief propagation returns  $r_{ji}^\alpha$  and  $q_{ji}^\alpha$ ,  $\forall \alpha, i, j$ . Then, the total a posteriori probability  $\Pr(l_i = \alpha)$  is computed as

$$\Pr(l_i = \alpha) = f_i^\alpha \prod_{j \in \mathcal{M}(i)} r_{ji}^\alpha, \quad (44)$$

and the total a posteriori probability of each label is given by

$$\Pr(\boldsymbol{l} = \{\alpha_1, \alpha_2, \dots, \alpha_m\}) = \prod_{i=1}^m \Pr(l_i = \alpha_i). \quad (45)$$

In Appendix I it is shown that when a lattice is represented by a Tanner graph, it is possible to associate a Markov process with the model for soft detection of lattice points, as shown in Fig. 3; also, that the extrinsic APPs  $P_k^{\text{BP}}(c^j; O)$  and  $P_k^{\text{BP}}(w^j; O)$  after belief propagation, corresponding to the  $k$ -th transition between states, can be computed as:

$$\begin{aligned} P_k^{\text{BP}}(c^j; O) &= \sum_{e: C_k^j(e)=c^j} \Pr(\boldsymbol{l}_{s^S(e)}) \prod_{i=1}^m P_k[u^i(e); I] \\ &\quad \times \prod_{i=1; i \neq j}^m P_k[c^i(e); I], \end{aligned} \quad (46)$$

$$\begin{aligned} P_k^{\text{BP}}(w^j; O) &= \sum_{e: U_k^j(e)=w^j} \Pr(\boldsymbol{l}_{s^S(e)}) \prod_{i=1; i \neq j}^m P_k[u^i(e); I] \\ &\quad \times \prod_{i=1}^m P_k[c^i(e); I], \end{aligned} \quad (47)$$

where  $\boldsymbol{l}_{s^S(e)}$  is the label indexed by the integer value of the starting state  $s^S(e)$  of edge  $e$ .  $P_k[u^i(e); I]$  and  $P_k[c^i(e); I]$  are the a priori probabilities of an unencoded, respectively encoded, symbol element (in this case a coordinate<sup>7</sup>) at position  $i$ , which are associated with edge  $e$  [16]. In a serial concatenation such as in Fig. 4, the unencoded symbol elements are assumed to be identically distributed according to a uniform distribution, and

<sup>5</sup>A *real* coordinate of a lattice point, not an *integer* coordinate of a label.

<sup>6</sup>The subscript  $k$ , which would indicate the time index of the relevant MIMO channel use, is omitted here and in Fig. 4 for simplicity of notation.

<sup>7</sup>I.e., not necessarily a binary symbol, or bit.

$P_k[u^i(e); I]$  is the reciprocal of the alphabet size at position  $i$ .  $P_k(c^i(e); I)$  are the likelihoods of lattice point coordinates, which can be computed as in the Tanner graph initialization step.

$$\forall \text{ edge } e, u(e) = \boldsymbol{\lambda} \in \Lambda(\mathbf{l}_i) \rightarrow \begin{cases} s^E(e) = i, i \in \{1, \dots, |\Lambda(\Lambda)|\} \\ \mathbf{c}(e) = \mathbf{u}(e) \end{cases}$$

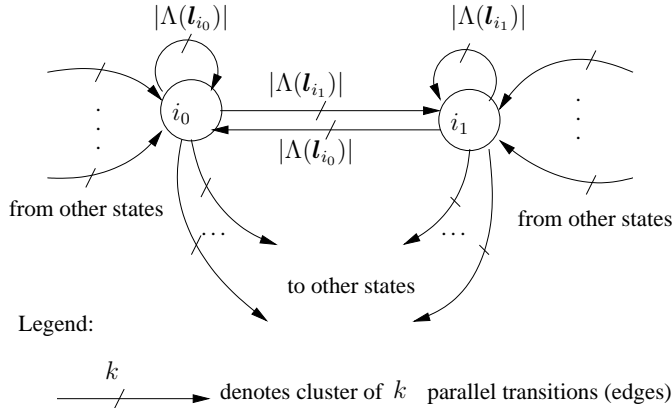


Fig. 3. State transition diagram for Markov process representing a sequence of lattice points. Edges occur in clusters because every label generally covers more than one point in the shaping region. States are label indices; the state at any time is the *index* of the label that contains the most recent lattice point output by the Markov source. When the Markov source outputs a new point it transitions into the state indexing the label that contains the new point.

#### IV. APPLICATION TO THE DETECTION OF SUPER-ORTHOGONAL LATTICE SPACE-TIME CODE

Consider the superorthogonal space-time code [2], [3], [4], [5], [6], [7] as the MIMO transmission scheme. The decoding algorithm developed in the previous section combined with hypothesis testing is introduced as an efficient MIMO detector.

##### A. Receiver for quasistatic scenarios

Consider the superorthogonal space-time code given in Example 2. The ML receiver for  $\mathbf{x}_\oplus$  is given by

$$\mathbf{x}_{\oplus;\text{ML}} = \arg \min_{\forall \mathbf{x}_\oplus} \|\mathbf{y} - \mathbf{H}_\oplus \mathbf{x}_\oplus\|^2. \quad (48)$$

The ML receiver is usually computationally complicated since it needs to examine all valid lattice points (complexity grows exponentially). The algorithm introduced in Section III offers a computationally efficient solution.

Recall that for a superorthogonal space-time code (see Example 2), either all  $\chi_l$  or all  $\chi_{l'}$  are zeros, which identifies two hypotheses: hypothesis  $H_1$  is that  $\chi_{l'}$  are all zeros, and the base matrices  $\mathbf{C}$  are chosen; hypothesis  $H_2$  is that  $\chi_l$  are all zeros, and the base matrices  $\mathbf{C}'$  are chosen. When hypothesis  $H_1$  is true, the transmission model (19) can be simplified as

$$\mathbf{y} = \mathbf{H}_\oplus^1 \boldsymbol{\chi} + \mathbf{n}. \quad (49)$$

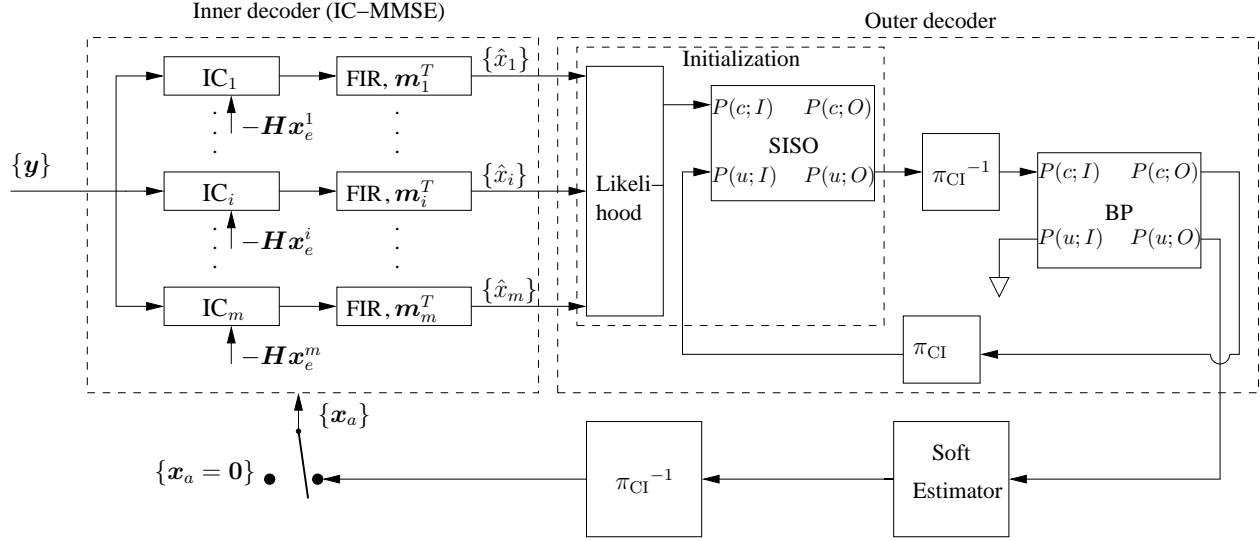


Fig. 4. The block diagram of the novel iterative receiver for super-orthogonal space-time lattice code in the presence of coordinator interleaver.

When hypothesis  $H_2$  is true, we have

$$\mathbf{y} = \mathbf{H}_{\oplus}^2 \boldsymbol{\chi}' + \mathbf{n}. \quad (50)$$

Due to the orthogonality of matrices  $\mathbf{H}_{\oplus}^k$ ,  $k = 1, 2$ , the MMSE filters for  $\boldsymbol{\chi}$ ,  $\boldsymbol{\chi}'$  are the corresponding matched filters

$$\mathbf{M}^k = \frac{1}{\alpha} \left( \mathbf{H}_{\oplus}^k \right)^H, \quad k = 1, 2 \quad (51)$$

where  $\mathbf{M}^k$  are MMSE filters for hypothesis  $H_k$ . The output of MMSE filters for hypothesis  $H_1$  and  $H_2$  are then given by

$$\hat{\boldsymbol{\chi}} = \mathbf{M}^1 \mathbf{y} = \frac{1}{\alpha} \left( \mathbf{H}_{\oplus}^1 \right)^H \mathbf{y} = \boldsymbol{\chi} + \tilde{\mathbf{n}}^1 \quad (52)$$

$$\hat{\boldsymbol{\chi}}' = \mathbf{M}^2 \mathbf{y} = \frac{1}{\alpha} \left( \mathbf{H}_{\oplus}^2 \right)^H \mathbf{y} = \boldsymbol{\chi}' + \tilde{\mathbf{n}}^2 \quad (53)$$

where  $\tilde{\mathbf{n}}^1$  and  $\tilde{\mathbf{n}}^2$  are estimation noise after filtering for hypothesis  $H_1$  and  $H_2$ , respectively. It is not difficult to see that  $\tilde{\mathbf{n}}^k$ ,  $k = 1, 2$  are white multivariate Gaussian random vectors, i.e.,  $\tilde{\mathbf{n}}^k \sim \mathcal{N}\left(0, \frac{N_0}{2\alpha} \mathbf{I}\right)$ . It should be pointed out that the IC is not necessary for this scenario and the estimations of (52),(53) are interference-free estimates of  $\boldsymbol{\chi}$  and  $\boldsymbol{\chi}'$ , respectively, due to the orthogonality of  $\mathbf{H}_{\oplus}^k$ .

The probability of hypothesis  $H_1$  given  $\mathbf{y}$  is:

$$\Pr(H_1 | \mathbf{y}) = \sum_{\boldsymbol{\chi}} \Pr(H_1, \boldsymbol{\chi} | \mathbf{y}). \quad (54)$$

In (54), summing over all valid values among  $\boldsymbol{\chi}$  becomes infeasible as the length of  $\boldsymbol{\chi}$  increases. In order to reduce the complexity, use the term that has the maximum value to approximate the summation (54). That is,

$$\Pr(H_1 | \mathbf{y}) \approx \max_{\boldsymbol{\chi}} \Pr(H_1, \boldsymbol{\chi} | \mathbf{y}) \sim p(\mathbf{y} | \mathbf{H}_{\oplus}^1, \boldsymbol{\chi}_{max}) \quad (55)$$

with

$$\begin{aligned}\chi_{max} &= \arg \max_{\chi} p(\mathbf{y}|\mathbf{H}_{\oplus}^1, \chi) = \arg \min_{\chi} |\mathbf{y} - \mathbf{H}_{\oplus}^1 \chi|^2 \\ &= \arg \min_{\chi} |\hat{\chi} - \chi|^2 = \text{sign}(\hat{\chi})\end{aligned}\quad (56)$$

where  $\hat{\chi}$  is the output of the LMMSE filtering for hypothesis  $H_1$  and is given in (52). Similarly,

$$\Pr(H_2|\mathbf{y}) \approx \max_{\chi'} \Pr(H_2, \chi'|\mathbf{y}) \sim p(\mathbf{y}|\mathbf{H}_{\oplus}^2, \chi'_{max}) \quad (57)$$

$$\chi'_{max} \stackrel{\text{def}}{=} \arg \min_{\chi'} |\mathbf{y} - \mathbf{H}_{\oplus}^2 \chi'|^2 = \text{sign}(\hat{\chi}'). \quad (58)$$

The log likelihood ratio of hypothesis  $H_1$  and  $H_2$  is

$$\begin{aligned}L(H) &= \log \frac{\Pr(H_1|\mathbf{y})}{\Pr(H_2|\mathbf{y})} \approx \log \frac{p(\mathbf{y}|\mathbf{H}_{\oplus}^1, \chi_{max})}{p(\mathbf{y}|\mathbf{H}_{\oplus}^2, \chi'_{max})} \\ &= \frac{2\alpha}{N_0} (\|\mathbf{y} - \mathbf{H}_{\oplus}^2 \chi'_{max}\|^2 - \|\mathbf{y} - \mathbf{H}_{\oplus}^1 \chi_{max}\|^2) \\ &= \frac{4\alpha}{N_0} (\mathbf{y}^H \mathbf{H}_{\oplus}^2 \chi'_{max} - \mathbf{y}^H \mathbf{H}_{\oplus}^1 \chi_{max}) \\ &= \frac{4\alpha^2}{N_0} (\hat{\chi}^H \chi_{max} - \hat{\chi}'^H \chi'_{max})\end{aligned}\quad (59)$$

Substituting (56) and (57) into (59) yields

$$L(H) = (\text{ABS}(\hat{\chi}) - \text{ABS}(\hat{\chi}')) 4\alpha^2/N_0 \quad (60)$$

where  $\text{ABS}(\mathbf{a}) = \sum |a_i|$ . Consequently, the probability of hypotheses  $H_1, H_2$  can be obtained from  $L(H)$

$$\Pr(H_k|\mathbf{y}) = 1/(1 + \exp(\mp L(H))), \quad k = 1, 2. \quad (61)$$

For each hypothesis one can apply the lattice detection algorithm developed in Section III for detecting  $\chi$ . We treat the information-bearing vector  $\chi$  as a lattice with generator matrix  $\mathbf{B}$ , i.e.,  $\chi = \mathbf{B}\mathbf{u}$ . For example, the equivalent model for detecting lattice point  $\chi$  is  $\hat{\chi} = \mathbf{B}\mathbf{u} + \tilde{\mathbf{n}}^1$ , where  $\hat{\chi}$  is the output of matched filtering of hypothesis  $H_1$ . Since  $\chi$  is from a  $D_4$  lattice, its generator matrix  $\mathbf{B}$  is given in (35). The APPs can be obtained according to Section III.

### B. Iterative receiver for coordinate interleaving in fast fading

Coordinate interleaving, along with the outer iteration loop in Fig. 4, is now considered; the real and imaginary parts of all complex symbols in a frame are collectively scrambled before transmission [18].  $\mathbf{Y} = \{\mathbf{y}_1, \mathbf{y}_2, \dots, \mathbf{y}_N\}$  denotes a frame spanning  $N$  MIMO channel uses at the MIMO channel output (before deinterleaving). Note that the structure of the superorthogonal lattice code is removed during transmission, and has to be recovered before detection. The applicable receive equation is (6) rather than (19); the iterative IC-MMSE attempts to iteratively remove the cross-antenna interference, i.e. to undo the channel  $\mathbf{H}$  on a per MIMO channel use basis. During the

first iteration, the soft feedback from the detector/decoder is null. The output of IC-MMSE is always deinterleaved, thus restoring the superorthogonal structure and yielding the soft-output  $\hat{\mathbf{X}} = \{\hat{\mathbf{x}}_1, \hat{\mathbf{x}}_2, \dots, \hat{\mathbf{x}}_N\}$  with

$$\hat{\mathbf{x}}_t = \mathbf{\Gamma} \chi_{\oplus;t} + \tilde{\mathbf{n}}_t. \quad (62)$$

Since the information-bearing vector  $\chi_{\oplus;t}$  is a direct sum of two  $D_4$  lattices, and the effective channel gain matrix  $\mathbf{\Gamma}$  is unitary, the equalization approach in Section IV-A applies to eq. (62).  $\Pr(H_k|\hat{\mathbf{x}}_t)$ ,  $k = 1, 2$ , are associated with the following transmission models upon removing  $\mathbf{\Gamma}_1$ ,  $\mathbf{\Gamma}_2$  respectively:

$$H_1 : \tilde{\chi}_t = \mathbf{B} \mathbf{u}_t + \tilde{\mathbf{n}}_t^1 \quad (63)$$

$$H_2 : \tilde{\chi}'_t = \mathbf{B} \mathbf{u}'_t + \tilde{\mathbf{n}}_t^2 \quad (64)$$

where  $\tilde{\chi}_t = \frac{1}{2} \mathbf{\Gamma}_1^T \hat{\mathbf{x}}_t$ ,  $\tilde{\chi}'_t = \frac{1}{2} \mathbf{\Gamma}_2^T \hat{\mathbf{x}}_t$ ,  $\tilde{\mathbf{n}}_t^1 = \frac{1}{2} \mathbf{\Gamma}_1^T \tilde{\mathbf{n}}_t$  and  $\tilde{\mathbf{n}}_t^2 = \frac{1}{2} \mathbf{\Gamma}_2^T \tilde{\mathbf{n}}_t$ . The generator matrix  $\mathbf{B}$  is given in (35). For each hypothesis, the lattice decoding algorithm can be applied to compute the extrinsic APPs  $P(u; O)$  and  $P(c; O)$ .

Inner-loop iterative decoding between SISO and BP, as shown in Fig. 4, can further improve the overall performance, especially in the presence of forward error correction coding, when decoding follows detection. Herein, only an uncoded system is considered in order to illustrate the concept. Even in an uncoded system it is possible to perform inner loop iterations between  $P^{\text{BP}}(c; O)$  from the belief propagation module and  $P(u; I)$  from the SISO block; more benefit is derived however when a decoder is part of the inner-loop.

## V. SIMULATIONS

Simulation results for a superorthogonal space-time lattice code with 4PSK constellation (Example 2), in both quasistatic and fast fading channels, are discussed. Each half of the superorthogonal constellation belongs to a  $D_4$  lattice, implicitly defining a shaping region; only six of the twelve  $L(\Lambda)$  labels listed in Example 3 (first four, last two) are needed to cover the lattice points in the shaping region. In order to test the algorithm's efficiency, only the most likely label (or two labels)—post belief propagation—are retained; the others receive zero probabilities (re-normalization is performed after setting to zero the probabilities of discarded labels).

### A. Quasistatic fading

The channel is constant over  $T = 2$  symbol periods. In our simulations, each data packet includes 500 super-orthogonal codewords. Each point on the curves plotted in Fig. 5 and Fig. 6 is obtained by testing 2000 independent data packets.

Fig. 5 shows the FER (frame error ratio)<sup>8</sup> vs.  $E_b/N_0$  for super-orthogonal space-time code when the coordinate interleaver is absent. QPSK modulation is employed and the channel spectral efficiency is 2.5 bits/channel use. The performance of the ML algorithm that exhaustively searches all possible valid codewords and picks the one with the ML is plotted as reference. For the MMSE-BP algorithm, we run one iteration for the Tanner graph and collect

<sup>8</sup>One frame is meant to be one super-orthogonal space-time codeword

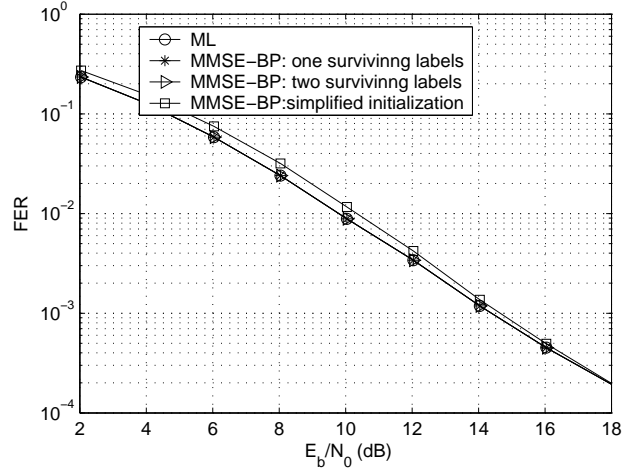


Fig. 5. FER vs.  $E_b/N_0$ ; super-orthogonal space-time lattice code, MMSE followed by BP. ML and BP with one and two surviving labels are identical. The curve with square markers illustrates the effect of simplified initialization.

the probability of the coordinate of label. Then we consider choosing one surviving label and two surviving labels. The simulation result shows that the MMSE-BP algorithm with one surviving label and two surviving labels have the same performance as that of the ML algorithm. The MMSE-BP with simplified initialization that reduces the overall complexity is also examined. In this case, we consider two surviving labels, the results show that it is about 0.5 dB away from the ML performance in low SNR region. As SNR increases, the MMSE-BP with simplified initialization approaches the ML performance asymptotically.

### B. Fast fading

Fast fading simulations include a coordinate interleaver. In our simulations, a depth-eight traditional block interleaver is considered. QPSK is used and the channel spectral efficiency is 2.5 bits/channel use. Two inner iterations are run between the SISO block and the BP block; one iteration is run on the lattice Tanner graph inside the BP block. We simulate different scenarios where different number of surviving labels are considered. In addition, iterative interference cancellation scheme is considered to improve the overall performance. The soft estimator computes the soft estimates of the coordinates of lattice point based on the output from the BP ( $P(u; O)$ ). Fig. 6 shows the FER vs.  $E_b/N_0$  for different number of surviving labels and different number of iterations between the IC-MMSE and the outer decoder.

## VI. CONCLUSION

A soft-output closest point search in lattices was introduced, via a form of belief propagation on a lattice. Due to the coding gain associated with a lattice, structural relations exist between certain lattice points, which can be associated via an equivalence relation for detection purposes. This leads to a soft-output detection algorithm, which

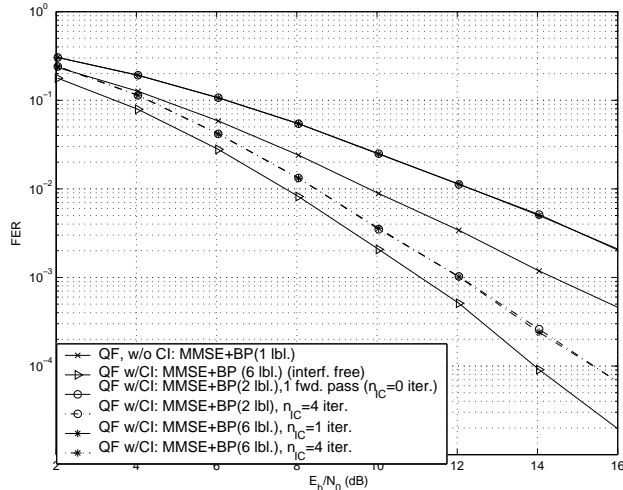


Fig. 6. FER vs.  $E_b/N_0$  of iterative decoding based on IC-MMSE plus BP for super-orthogonal space-time lattice code with coordinate interleaver.

can generate both total and extrinsic *a posteriori* probability at the detector’s output. The step-back feature of classic sphere decoding is eliminated.

APPENDIX I

COMPUTING THE EXTRINSIC A POSTERIORI PROBABILITIES AFTER BELIEF PROPAGATION

Herein, the expressions for extrinsic *a posteriori* probabilities (46), (47), at the belief propagation detector’s output, are derived; the extrinsic probabilities are needed in iterative receivers. Here, the goal of detection is to provide soft information about valid channel alphabet symbols, i.e. real coordinates of the complex symbols from the modulation constellations used on various transmit antennas; this information about coordinates can be used to revert the effect of a coordinate interleaver, or can be forwarded directly to a soft decoder for some coded modulation encoder. Alternatively, it can be used for soft or hard demodulation, e.g. in the case of bit interleaved coded modulation, or with plain uncoded transmission.

When a lattice is represented by a Tanner graph, it is possible to associate a Markov process with the model for soft detection of lattice points in a natural way. This is enabled by first viewing the sequence of lattice points passed through the channel as a Markov source. Another observation is that, in general, simple detection (with or without soft information) is by itself memoryless; thereby, one should expect the Markov process to be somehow degenerated, in order to reflect the memoryless nature of simple (non-iterative) detection. The objective of detection is to determine the *a posteriori* (total or extrinsic) probabilities of the output of the Markov source. In order to leverage off of known results—even in the case of plain, uncoded transmission (no forward error correcting redundancy added by encoding)—one can view the output  $c$  of the Markov source (a lattice point, i.e. a vector of lattice coordinates) as the result of mapping with rate one (i.e. no additional redundancy) an identical replica of

the input  $\mathbf{u} = \mathbf{c}$ ; this is a degenerated Markov process where even the dependence of the future on the present is removed. The only remaining structure to be captured for the Markov source, in the case when the candidate points are from a lattice, must reflect the partitioning in labeled cosets, as discussed in Section III-B. To this end, note that the labels themselves can be associated with states having integer values by virtue of the following convention: the state  $S_{k-1}$  at time  $k-1$  is the *index* of the label that contains the most recent lattice point output by the Markov source, i.e. at time  $k-1$ ; when the Markov source outputs a new point at time  $k$  it transitions into state  $S_k$  equal to the integer indexing the label that contains the new point. Alternatively, with respect to the mapping  $\mathbf{u} \mapsto \mathbf{c}$  and omitting the time index, when  $\mathbf{u} = \boldsymbol{\lambda} \in \Lambda$  occurs at the rate-one block input, the Markov process transitions into the state whose (integer) value indexes the label containing  $\boldsymbol{\lambda}$ . This is represented in Fig. 3, where  $e$  denotes an edge between starting state  $s^S(e)$  and ending state  $s^E(e)$ . Formally, for any edge  $e$ , at any time, if  $\mathbf{u}(e) = \boldsymbol{\lambda} \in \Lambda(\mathbf{l}_i) \subset \Lambda$ , where  $i \in \{1, \dots, |L(\Lambda)|\}$  indexes one of the  $|L(\Lambda)|$  labels, then the ending state  $s^E(e) = i$  and the Markov source outputs  $\mathbf{c}(e) = \mathbf{u}(e)$ . There is a bijective mapping  $\ell$  between integer states and labels  $s \mapsto \mathbf{l}_s$  such that, for any integer state  $s \in \{1, \dots, |L(\Lambda)|\}$ ,  $\ell(s) \stackrel{\text{def}}{=} \mathbf{l}_s$  is the label associated with  $s$ .

The Markov sequence of random points selected from the lattice can be thus viewed as triggered by state transitions triggered by  $\mathbf{u} = \boldsymbol{\lambda} \in \Lambda$ ; although the realizations of  $\mathbf{u}$  on the lattice grid are random, a state model arises as a result of partitioning the lattice in equivalence classes. That is, there exist certain structural relations between certain points, which can be associated via an equivalence relation. The state probabilities, used in a posteriori probability calculations, are seen to be associated with the probabilities of these equivalence classes (or their labels), which can be obtained separately from belief propagation on the lattice's Tanner graph, as shown next.

In general, for a Markov process generated by triggering state transitions via some input (e.g. a classical convolutional code), the new state depends on the current input and several previous inputs; in the case at hand the new state depends only on the current input. This illustrates the degenerated nature of the Markov process at hand, seen thereby to be memoryless.

The memoryless nature of the Markov process is also apparent in the fact that any state can be reached in one transition from any state, and the probability distribution of the states does not depend on time; it depends only on the probability distribution for  $\mathbf{u}$ , and so does the probability distribution of the output of the Markov process. The output of the Markov process does not depend on the current state, but rather on the input  $\mathbf{u}$ ; the input determines both the new output and the new state, which implies that the output any time does not depend on any previous state.

The remainder of this appendix will use the state transition diagram in Fig. 3 for the Markov process that forms the object of detection; the results in [16], [17] apply. Following [16], the extrinsic APPs  $P_k^{\text{BP}}(\mathbf{c}^j; \mathcal{O})$  and  $P_k^{\text{BP}}(\mathbf{u}^j; \mathcal{O})$  during the  $k$ -th transition between states have the general expressions

$$\begin{aligned}
 P_k^{\text{BP}}(\mathbf{c}^j; \mathcal{O}) &= \sum_{e: C_k^j(e) = \mathbf{c}^j} A_{k-1}[s^S(e)] \prod_{i=1}^m P_k[u^i(e); I] \\
 &\quad \times \prod_{i=1; i \neq j}^m P_k[\mathbf{c}^i(e); I] B_k[s^E(e)], \tag{65}
 \end{aligned}$$

$$\begin{aligned}
 P_k^{\text{BP}}(u^j; O) &= \sum_{e: U_k^j(e)=u^j} A_{k-1}[s^S(e)] \prod_{i=1; i \neq j}^m P_k[u^i(e); I] \\
 &\times \prod_{i=1}^m P_k[c^i(e); I] B_k[s^E(e)], \tag{66}
 \end{aligned}$$

where  $A_{k-1}[s^S(e)]$  and  $B_k[s^E(e)]$  are the probabilities of the current state and the new state that are associated with edge  $e$ . Following the well-known results and notation in [17] and using the memoryless nature of the Markov process in Fig. 3,

$$\begin{aligned}
 A_k[s] &\stackrel{\text{def}}{=} \Pr\{S_k = s; \mathbf{y}_1^k\} = \Pr\{S_k = s; \mathbf{y}_k; \mathbf{y}_1^{k-1}\} \\
 &= \Pr\{S_k = s; \mathbf{y}_k | \mathbf{y}_1^{k-1}\} \Pr\{\mathbf{y}_1^{k-1}\} \tag{67}
 \end{aligned}$$

$$= \Pr\{S_k = s; \mathbf{y}_k\} \Pr\{\mathbf{y}_1^{k-1}\} = \Pr\{S_k = s; \mathbf{y}_k\} \kappa_0, \tag{68}$$

where, following [17],  $\mathbf{y}_0^\tau$  denotes the observations of the relevant Markov process, as taken at the output of a discrete memoryless channel at time instants  $0, 1, \dots, \tau$ . Most importantly, the factor  $\kappa_0$  does not depend on the state  $s$ , and is thereby cancelled out during the normalization step that enforces  $\sum_s A_k[s] = 1$ . Due to the isomorphism between states and labels it follows that  $\Pr\{S_k = s; \mathbf{y}_k\}$  is the label probability  $\Pr(\ell(s)) = \Pr(\mathbf{l}_s)$  calculated as in (45). From [17] and the properties of the degenerated Markov process,

$$B_k[s] \stackrel{\text{def}}{=} \Pr\{\mathbf{y}_{k+1}^\tau | S_k = s\} = \Pr\{\mathbf{y}_{k+1}^\tau\}, \tag{69}$$

which does not depend on the state  $s$  and behaves as a constant that is cancelled out during the normalization step enforcing  $\sum_s B_k[s] = 1$ . Therefore (46), (47) follow.

## REFERENCES

- [1] A. H. Banihashemi and I. F. Blake, "Trellis structure and decoding complexity of lattices," Ph. D. dissertation, ECE Dept., Univ. Waterloo, Waterloo, ON, Canada, 1997
- [2] D. M. Ionescu, K. K. Mukkavilli, Z. Yan, and J. Lilleberg, "Improved 8- and 16-State Space-Time codes for 4PSK with Two Transmit Antennas," *IEEE Commun. Letters*, vol. 5, pp. 301–303, July 2001.
- [3] S. Siwamogsatham and M. P. Fitz, "Improved High-Rate Space-Time Codes via Concatenation of Expanded Orthogonal Block Code and M-TCM," *Proceedings of 2002 ICC*, vol. 1, pp. 636–640, May 2002.
- [4] S. Siwamogsatham and M. P. Fitz, "Improved High-Rate Space-Time Codes via Orthogonality and Set Partitioning," *Proceedings of 2002 IEEE WCNC*, vol. 1, pp. 264–270, March 2002.
- [5] N. Seshadri and H. Jafarkhani, "Super-Orthogonal Space-Time Trellis Codes," *Proc. ICC'02*, May 2002, Vol. 3, pp. 1439–1443.
- [6] H. Jafarkhani, N. Seshadri, "Super-orthogonal space-time trellis codes," *IEEE Trans. Inform. Theory*, vol. 49, pp. 937–950, Apr. 2003.
- [7] D. M. Ionescu and Z. Yan, "Fading-Resilient Super-Orthogonal Space-Time Signal Sets: Can Good Constellations Survive in Fading?," submitted to *IEEE Trans. Inform. Theory*; available on the ArXiv server <http://www.arxiv.org/abs/cs.IT/0505049>
- [8] O. Tirkkonen and A. Hottinen, "Square-matrix embeddable space-time block codes for complex signal constellations," *IEEE Trans. Inform. Theory*, vol. 48, pp. 384–395, Feb. 2002.
- [9] Z. Yan and D. M. Ionescu, "Geometrical Uniformity of a Class of Space-Time Trellis Codes," *IEEE Trans. Inform. Theory*, vol. 50, pp. 3343–3347, Dec. 2004.
- [10] H. El Gamal, G. Caire, M. O. Damen, "Lattice coding and decoding achieve optimal diversity-multiplexing tradeoff of MIMO channels," *IEEE Trans. Inform. Theory*, vol. 50, no. 6, pp. 968–985, June 2004.
- [11] B. Hassibi and B. M. Hochwald, "High-rate codes that are linear in space and time," *IEEE Trans. Inform. Theory*, vol. 48, no. 7, pp. 1804–1824, July 2002.

- [12] B. Farhang-Boroujeny, *Adaptive Filters: theory and applications*. Chichester, West Sussex, England: Wiley, 2000.
- [13] A. H. Banihashemi and F. R. Kschischang, “Tanner graphs for group block codes and lattices: construction and complexity,” *IEEE Trans. Inform. Theory*, vol. 47, Feb 2001
- [14] M. C. Davey and D. MacKay, “Low-Density Parity Check Codes over  $GF(q)$ ,” *IEEE Commun. Letters*, vol. 2, June 1998
- [15] E. Agrell, T. Eriksson, A. Vardy, and K. Zeger, “Closest point search in lattices,” *IEEE Trans. Inform. Theory*, vol. 48, No. 2, pp. 2201-2214, Aug. 2002.
- [16] S. Benedetto, D. Divsalar, G. Montorsi, and F. Pollara, “A soft-input soft-output APP module for iterative decoding of concatenated codes,” *IEEE Commun. Lett.*, vol. 1, pp. 22–24, Jan. 1997.
- [17] L. R. Bahl, J. Cocke, F. Jelinek, and J. Raviv, “Optimal decoding of linear codes for minimizing symbol error rate,” *IEEE Trans. Inform. Theory*, vol. IT-20, pp. 284-287, Mar. 1974.
- [18] D. M. Ionescu, D. Doan, S. Gray, “On Interleaving Techniques for MIMO Channels and Limitations of Bit Interleaved Coded Modulation,” submitted to *IEEE Trans. Inform. Theory*; available on the ArXiv server <http://www.arxiv.org/abs/cs.IT/0510072>.